Large Magnetooptical Kerr Rotation with High Reflectivity from Photonic Bandgap Structures with Defects

M. J. Steel, M. Levy, and R. M. Osgood, Jr., *Fellow, IEEE*

***Abstract*—We perform a theoretical study of enhancement of magnetooptical rotation on reflection of light from a periodic system with a defect. Using calculations based on a coupled mode approach and the transfer matrix method we demonstrate that an asymmetric placing of a single defect allows arbitrary Kerr rotations with better than 99% reflectivity from very short devices.**

***Index Terms*—Defect, Faraday rotation, Kerr rotation, magnetooptical rotation, periodic structure, photonic crystal, transmission resonance.**

I. Introduction

MAGNETOOPTICAL rotation is most commonly associated with Faraday rotation—the rotation of plane polarized light on *transmission* through a magnetic medium due to magnetic circular birefringence. However, the analogous rotation obtained by reflection from a magnetic medium, known as the Kerr effect, is also important. Well-known applications include the characterization of thin films, and information read out from magnetooptical disks. A variety of dielectric materials exhibit magnetooptical rotation. In integrated optics, a notable example is bismuth-substituted yttrium iron garnet (Bi-YIG) due to its comparatively strong rotation, low loss, and its suitability for heterogeneous integration by single-crystal liftoff and direct bonding [1] or sputtering. Due to the small interaction lengths on reflection, Kerr rotations are normally small compared to Faraday rotations, and while Bi-YIG has a higher rotation per loss than most materials, Kerr rotations of only fractions of a degree are typical. For a number of applications, it would thus be useful to extract larger Kerr rotations.

Recently, there have been several studies of the enhancement of magnetooptical rotation in periodic systems with defects [2]–[6] (and also in random structures [7]). Periodic systems such as thin-film stacks, fiber Bragg gratings [8], and photonic crystals [9], are, of course, characterized by the existence of photonic bandgaps (PBGs)—frequency bands in which incident light is strongly reflected. The addition of defects to periodic structures leads to the creation of transmission resonances associated with trapped states—a familiar example is distributed feedback lasers constructed from a dielectric stack with a central π phase shift. The essential finding of this work [2]–[4] is that these systems can produce both Faraday and Kerr rotations far larger than possible for comparable uniform systems. The enhancement operates in the following basic fashion [5]. The structure is illuminated with linearly polarized light at or close to the frequency of an in-bandgap resonance associated with the defect(s). The light is trapped inside, localized in the vicinity of the defects, with a consequent increase in the mean optical path length of the emitted light. As the mean path length grows, there is also an increase in the optical path *difference* between the two equally excited circularly polarized modes as the magnetic circular birefringence acts over a longer path. The emitted light thus suffers a larger rotation.

In this way, propagation lengths for a given rotation may be reduced greatly—Faraday rotations of 45° or more are predicted for lengths of a few tens of micrometers, and experiments have confirmed the effect with observation of both Faraday and Kerr rotations in excess of 10° at visible wavelengths, from stacks of only $\approx$10 μm in length [3]. However, the structures initially studied, which have a single central defect, are far from optimal because the observed rotation decreases with the intensity of the output light. In other words, the transmissivity is small when the Faraday rotation is large, and the reflectivity is small when the Kerr rotation is large. Indeed, the largest Kerr rotations in the experiments were achieved with reflectivities less than 1%.

In an earlier paper [5], we introduced a coupled-mode description to study enhancement in the Faraday (transmission) case. It was shown that the tradeoff associated with a single central defect was unavoidable, but that using two defects placed appropriately, the structure contained sufficient degrees of freedom to obtain both high output and high rotations. Such improved performance with multiple defects was initially predicted for a certain limited class of designs in [4]. However, the improvements were unexplained and did not allow high transmission for all angles. Our own work [5] explained the improved transmission and considered a broader class of structures so that high transmission was possible for a very large range of rotations.

In this paper, we continue this study by turning to the optimization of Kerr rotation. We again overcome the tradeoff between rotation and reflectivity by introducing an extra degree of freedom to the design; in this case, by exploring

Manuscript received January 13, 2000. This work was supported in part by DARPA/AFOSR under Contract F49620-99-1-0038, and in part by an NIST Advanced Technology Program under NIST Cooperative Agreement 70NANB8H4018.

The authors are with the Department of Applied Physics and Columbia Radiation Laboratory, School of Engineering and Applied Sciences, Columbia University, New York, NY 10027 (e-mail: mikes@cumsl.ctr.columbia.edu).

Publisher Item Identifier S 0733-8724(00)08073-7.

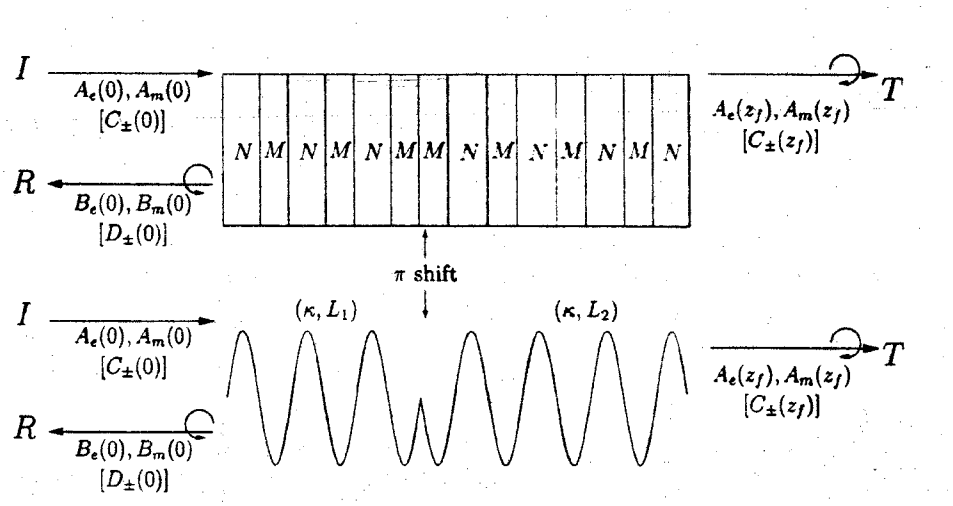

Fig. 1. Connection between thin-film stack and coupled-mode formalism. The upper panel shows a quarter-wave stack $(NM)^3(MN)^4$ of materials with refractive indexes M and N and the lower panel, a schematic representation of the corresponding coupled-mode picture. The incoming and outgoing fields are also indicated for both linear $(A_e,\ A_m,\ B_e,\ B_m)$ and the corresponding circular polarizations $(C_\pm,\ D_\pm)$.

asymmetric structures. It is particularly easy to optimize such designs because different parts of the structure are largely separately responsible for the two aims of high reflection and high rotation.

The paper is structured as follows. In Section II, we review the essential points of the model presented in [5]. In Section III, we briefly explain the tradeoff observed for symmetric structures. Section IV shows that asymmetric structures escape this tradeoff and we examine the performance of a number of designs using both the coupled-mode theory and the transfer-matrix method. We show that our designs permit rotation over the entire range 0°–90° with essentially 100% reflection.

II. Summary of Mathematical Model

A. Coupled-Mode Description

In this section, we summarize the main points of our coupled-mode description, which was developed in [5] and to which the reader is referred for details. Fig. 1 shows the basic geometry. Incoming linearly polarized light (I) is incident on a quarter-wave stack (upper half of Fig. 1) or general periodic system (lower half) that contains one or more isolated defects separating strictly periodic regions. The defects consist of a missing layer or π phase slip in the periodicity. The object is to calculate the reflection and transmission coefficients R and T and the degree of rotation and ellipticity of the emitted light. We denote the front of the stack by $z = z_0$ and the rear by $z = z_f$.

We assume an external magnetic field is applied in the longitudinal (z) direction to saturate the magnetic material. In a magnetic layer, the dielectric tensor then has nonvanishing off-diagonal elements $\epsilon_{xy} = -\epsilon_{yx} = i\epsilon_o$, while in nonmagnetic layers, it is assumed isotropic. To obtain a coupled-mode description, the dielectric tensors for the individual layers are replaced by an approximate Fourier expansion in each periodic section

$$\overleftrightarrow{\epsilon} = \begin{bmatrix} [\bar{\epsilon}_d + \epsilon'_d g(z)], & i[\bar{\epsilon}_o + \epsilon'_o g(z)], & 0 \\ -i[\bar{\epsilon}_o + \epsilon'_o g(z)], & [\bar{\epsilon}_d + \epsilon'_d g(z)], & 0 \\ 0, & 0, & \epsilon_{zz} \end{bmatrix}. \quad (1)$$

Here $g(z) = \cos[(2\pi z/\Lambda) + \delta]$, Λ is the stack period, and δ varies from one section to the next to account for the phase shift. To date, work on magnetooptical rotation in such structures has concentrated on one-dimensional (1-D) thin-film stacks, but consideration of corrugated waveguides [5] or 1-D photonic crystal devices would also be possible. For a corrugated waveguide, (1) is interpreted as a description of the *effective* dielectric tensor of the device. Note that we do not include dispersion between the transverse electric [TE](x) and transverse magnetic [TM] (y) modes, as significant dispersion inhibits the magnetooptical rotation through phase mismatch [5] and would destroy the effects we wish to discuss. In a waveguide geometry, the structure would have to be designed to minimize dispersion.

The electric field at wavelength $\lambda = 2\pi c/\omega$ is written

$$\begin{aligned} \boldsymbol{E} = \{&[A_e(z)\boldsymbol{v}_e + A_m(z)\boldsymbol{v}_m]\exp(i\pi z/\Lambda) \\ &+ [B_e(z)\boldsymbol{v}_e + B_m(z)\boldsymbol{v}_m]\exp(-i\pi z/\Lambda)\} \\ &\cdot \exp(-i\omega t) + c.c. \end{aligned} \quad (2)$$

where $\boldsymbol{v}_{e,m}(x, y)$ are the normalized mode functions for TE (e) and TM (m) modes, which for a stack geometry reduce to plane waves with $\hat{\boldsymbol{x}}$ and $\hat{\boldsymbol{y}}$ polarization. Equations (1) and (2) are substituted into the Maxwell wave equation and nonphase-matched terms discarded to obtain the coupled-mode equations. As shown in [5], the problem is best expressed in terms of the circular polarization modes

$$C_\pm = (A_e \mp iA_m)/\sqrt{2} \quad (3a)$$

$$D_\pm = (B_e \mp iB_m)/\sqrt{2}. \quad (3b)$$

With the assumption of degeneracy between the TE and TM modes, the coupled-mode system separates into pairs of equations for the mode pairs (C_+, D_+) and (C_-, D_-), which each satisfy the well-known equations for a periodic structure

$$\frac{d}{dz}\begin{bmatrix} C_\pm \\ D_\pm \end{bmatrix} = \mathsf{U}^\pm \begin{bmatrix} C_\pm \\ D_\pm \end{bmatrix} = i\begin{bmatrix} q_\pm & \kappa_\pm e^{i\delta} \\ -\kappa_\pm e^{-i\delta} & -q_\pm \end{bmatrix}\begin{bmatrix} C_\pm \\ D_\pm \end{bmatrix}. \tag{4}$$

The quantities $q_\pm = q \pm \alpha_0$, where $q = (\omega - \omega_0)\overline{n}/c$ represent detunings from the resonant Bragg frequency ω_0 and contain a contribution from the mean index $\overline{n}$ and mean magnetic strength $\alpha_0 = \pi\epsilon_o/(\overline{n}\lambda)$. Note that $\omega_0 = 2\pi c/\lambda_0$, with $\lambda_0 = 2\overline{n}\Lambda$. Similarly, the grating coupling strengths $\kappa_\pm = \kappa \pm \alpha_1$ depend on both the periodicity in the index profile through $\kappa = (n_2 - n_1)/(\overline{n}\Lambda)$ and the periodic part of the magnetic terms $\alpha_1 = \pi\epsilon_o'/(\overline{n}\lambda)$. Note that the signs of α_0 and α_1 depend on the direction of the applied magnetic field.

In solving (4), we use (3) to apply the boundary conditions $A_e(0) = 1$ and $A_m(0) = B_e(z_f) = B_m(z_f) = 0$, representing a single TE (x polarized) input of unit amplitude at the front of the structure (see Fig. 1).

B. One-Defect Systems

In this paper, we concentrate on structures with a single phase shift separating two periodic gratings (more complex structures were treated in [5]). We denote such a structure as $(\kappa_1, L_1):(\kappa_2, L_2)$ indicating the coupling strength κ_j and length L_j of each section. To precisely describe a corresponding thin-film stack we write expressions of the form $(MN_1)^l(N_2M)^m$, where M denotes a magnetic layer and N_j a nonmagnetic layer. [These stack structures are solved by the transfer matrix method [2], [4], [10], with all layers being quarter-wave plates of thickness $t = \lambda_0/(4n_j)$.] The relation between the two pictures is indicated schematically in Fig. 1.

The solution for a stack with a single defect separating periodic sections of length L_1 and L_2 is simply

$$\begin{bmatrix} C_\pm \\ D_\pm \end{bmatrix}_{z=z_f} = e^{\mathsf{U}_2^\pm L_2} e^{\mathsf{U}_1^\pm L_1}\begin{bmatrix} C_\pm \\ D_\pm \end{bmatrix}_{z=z_0} \tag{5}$$

where the phase δ differs by π in the matrices $\mathsf{U}_1^\pm$ and $\mathsf{U}_2^\pm$. From the reflection $(r_\pm)$ and transmission $(t_\pm)$ coefficients for the individual circular polarizations

$$r_\pm = |r_\pm|e^{i\psi_\pm} = \frac{D_\pm(0)}{C_\pm(0)} \tag{6}$$

$$t_\pm = |t_\pm|e^{i\phi_\pm} = \frac{C_\pm(z_f)}{C_\pm(0)} \tag{7}$$

combined with (3), we can find the main parameters of interest: the total transmission and reflection coefficients

$$T = |A_e(z_f)|^2 + |A_m(z_f)|^2 \qquad R = |B_e(0)|^2 + |B_m(0)|^2 \tag{8}$$

and the Faraday and Kerr rotations θ_F, θ_K, and corresponding ellipticities η_F and η_K, defined as

$$\theta_{F,K} = \frac{1}{2}\tan^{-1}\frac{2\,\mathrm{Re}(\chi_{F,K})}{1 - |\chi_{F,K}|^2} \tag{9}$$

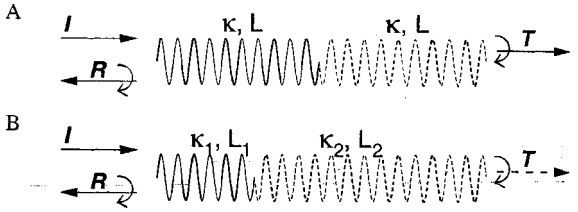

Fig. 2. Schematic of structures considered: A–Single symmetric defect. B–Single asymmetric defect. The dashed lines in each structure are used only to highlight the phase shifts. Our interest is in optimizing the reflection R for Structure B.

$$\eta_{F,K} = \tan\left[\frac{1}{2}\sin^{-1}\left(\frac{-2\,\mathrm{Im}(\chi_{F,K})}{1 + |\chi_{F,K}|^2}\right)\right] \tag{10}$$

where $\chi_F = A_m(z_f)/A_e(z_f)$ and $\chi_K = B_m(0)/B_e(0)$. For the special case that $|r_+| = |r_-|$, it is easy to show that the ellipticity vanishes $(\eta_K = 0)$ and that

$$\theta_K = -(\psi_+ - \psi_-)/2. \tag{11}$$

This is an important relation. Similarly, if $|t_+| = |t_-|$, we have $\eta_F = 0$ and

$$\theta_F = -(\phi_+ - \phi_-)/2. \tag{12}$$

C. Summary of Effects

Equation (4) indicates that in a uniform structure (no defects), each pair of circularly polarized modes (C_+, D_+) and (C_-, D_-) exhibits a PBG, centered at the points $q_\pm = 0$, respectively, due to the periodicity. Light of frequencies inside the bandgap is strongly reflected by the structure with a peak reflectivity $\tanh^2(\kappa_\pm L)$. The magnetic circular birefringence resulting from the average magnetooptical strength induces a small splitting $q_+ - q_- = 2\alpha_0$ in the location of the bandgaps. Due to the periodic magnetic term α_1, the reflectivities for opposite polarizations are also slightly different, though as we explain later, this effect can be neglected in the present case. Once the problem is solved for the individual circular components, the total response expressed in terms of linear polarizations is easily found by summing the components using (3).

Equation (5) describes the response when a phase shift or defect is introduced into the system (see Figs. 1 and 2). The principal effect of adding one or more phase shifts is the introduction of narrow transmission resonances near the center of the bandgaps. In general, the width of the bandgaps $2\kappa_\pm \gg \alpha_0$, α_1, and the magnetic effects are regarded as a perturbation to the grating. However, the bandwidth of the *defect resonances* can be comparable to α_0 and, as we see below, the two effects can interact strongly to produce enhancement.

D. Physical Units

Our calculations are performed for thin-film stacks constructed of either bismuth-substituted YIG (Bi-YIG) and GGG, or Bi-YIG and SiO_2, for higher contrast devices We also show results for corrugated Bi-YIG waveguides on a GGG substrate. The diagonal elements of the dielectric tensors of these materials are $\epsilon_{xx}^{\mathrm{YIG}} = 4.75$, $\epsilon_{xx}^{\mathrm{GGG}} = 3.71$, and $\epsilon_{xx}^{\mathrm{SiO_2}} = 2.25$. The off-diagonal element for Bi-YIG is $\epsilon_{xy} = 0.00269$ which

corresponds to a Faraday rotation of $\theta_F = 0.48^\circ\ \mu\text{m}^{-1}$. We assume a resonant frequency of $\lambda_0 = 1.55\ \mu$m.

We frequently use dimensionless units in which all parameters are scaled by the intrinsic rotation per unit length of the magnetic material: $\gamma_0 = \pi\epsilon_{xy}/(\overline{n}\lambda_0)$. For YIG/GGG stacks, $\gamma_0 = 0.00266\ \mu\text{m}^{-1}$ and the main parameters take the values $\alpha_0 = 0.47$, $\alpha_1 = 0.626$, and $\kappa = 123$ [6].

III. Symmetric Structures

To date, most attention has focused on enhancement of magnetooptical rotation in highly symmetric structures [2]–[4] (though Inoue *et al.* have also examined random multilayers.) The simplest example is a strictly alternating stack of magnetic and nonmagnetic layers with a single layer removed in the exact center (see Structure A in Fig. 2). An alternative but similar scheme is to place a single magnetic layer at the center of a nonmagnetic stack in the form $(N_1N_2)^m(M)(N_2N_1)^m$. This latter type was used in experiments [3]. Both transfer-matrix models and experiments showed that when tuned to the transmission resonances of these structures, transmitted and reflected light exhibited highly enhanced rotations. As mentioned earlier, however, the enhancement is associated with a substantial decrease in the output intensity, with an increasing penalty in intensity as the rotation increases. In [5], we used the coupled mode theory to explain this trade-off and showed that it is unavoidable for the single-defect symmetric system. Indeed the rotation and output were shown to be connected by the simple relations

$$T = \cos^2\theta_F \qquad R = \cos^2\theta_R \tag{13}$$

so that large rotations $\gtrsim 45^\circ$ imply low output intensities.

The reason for this tradeoff may be understood physically from Fig. 3(a) and (b). The mathematical description is available in [5]. Our discussion is framed for operation in transmission, but the reflection problem is exactly analogous. Fig. 3(a) shows the transmission coefficients $T_\pm = |t_\pm|^2$ for Structure A with YIG/GGG parameters for a length $L = 9.5\ \mu$m. The transmission resonances at the center of the bandgap are clearly apparent, though the splitting is hardly visible on this scale. The upper panel of Fig. 3(b) shows a blowup of the resonances indicating the splitting of the two modes, and also includes the associated phase profiles $\phi_\pm$ (dotted lines). The lower panel shows the same situation but expressed in terms of linear polarizations.

First we study the circular modes in the upper panel of Fig. 3(b). In order to achieve a zero ellipticity, we require $|t_+| = |t_-|$, which occurs at $q = 0$. The phase profiles $\phi_\pm$ have the form of smoothed step functions and naturally exhibit the same magnetic splitting as the intensity profiles. As a result, there is a considerable phase difference $\phi_+ - \phi_-$ (denoted by the vertical arrow), which via (12) corresponds to a Faraday rotation. This is apparent in the corresponding linear polarization panel below. At $q = 0$, a significant fraction of the transmitted energy is TM polarized. In fact, the Faraday rotation $\theta_F \approx 41^\circ$. However, it is also apparent that the total transmission $T(q=0) = |A_e(z_f)|^2 + |A_m(z_f)|^2$ is only ≈ 0.55, consistent with the transmission of the circular modes at $q = 0$.

Now consider the behavior as the strength κL of each grating is increased. Increasing the grating strength also increases the quality Q or energy storage of the transmission resonances, and, therefore, the linewidth of the resonances must decrease. From the upper panel of Fig. 3(b), we see that this would reduce the transmission of each of the circular modes at $q = 0$ and so the total transmission is reduced. On the other hand, the phase profiles $\phi_\pm$ must also follow the decrease in linewidth, and hence they grow more step-like with increasing length. The phase difference at $q = 0$ and thus the Faraday rotation, therefore, increase, tending toward $\theta_F = 90^\circ$, as the bandwidth and transmission tend to zero. An exactly analogous argument can be made for rotation of the reflected light. Thus the behavior is in accord with (13).

With the assumption of a symmetric structure, there are no available degrees of freedom other than the grating strength κL and we conclude that the tradeoff is inescapable.

IV. Asymmetric Structures

In [4], it was shown that for Faraday rotation, certain stack designs containing two defects could achieve higher transmission while still maintaining enhanced rotations. We subsequently performed a systematic study of two defect systems [5], [6], explaining how the defects should be placed in order to attain high transmission ($\approx 99^\circ$) for essentially any desired rotation. The improvement results from the additional degree of freedom introduced by the second defect, which permits an accidental degeneracy between two resonance peaks of opposite parity.

Here, we aim to optimize Kerr rotation and again seek to introduce an extra degree of freedom in order to overcome the tradeoff occurring in the symmetric single-defect structures. In this case, our answer is not to introduce a second defect, but to use an asymmetric placement of the single defect. Consider the effect of moving the central defect in Structure A (Fig. 2) toward the front of the stack (Structure B). We also allow the rear coupling strength to be larger so that we have the structure $(\kappa_1, L_1) : (\kappa_2, L_2)$ with $\kappa_2 \geq \kappa_1$. It is to be expected that the reduction in symmetry affects the transmission resonance. Indeed, (5) is easily solved to give the peak transmission

$$T_\pm \equiv |t_\pm(q_\pm = 0)|^2 = \frac{1}{\cosh^2(\kappa_2 L_2 - \kappa_1 L_1)} \tag{14}$$

so that the structure is essentially opaque, once $\kappa_2 L_2 - \kappa_2 L_2 \gtrsim 3$–$4$. Compared to the front grating, the rear grating may then be regarded as an essentially perfect reflector, and the reflection spectrum is featureless and close to unity throughout the bandgap. However, as we see below, whereas the transmission at the former resonance vanishes, a signature of the defect remains in the form of a rapid variation in the phase profiles of the reflected light $\psi_\pm = \arg(r_\pm)$. These profiles induce a large phase difference and rotation, just as was found for the transmission phases $\phi_\pm$ in the symmetric case of Fig. 3. However, as the rear grating strength significantly exceeds that of the first, the light must be highly reflected and we succeed in breaking the rotation-intensity tradeoff in Kerr mode.

In evaluating the properties of such asymmetric structures, we consider two types of systems that differ in the distribution of magnetic layers. Type I systems have the same materials on both sides of the defect, i.e., stacks of the form $(NM)^j(MN)^k$, with

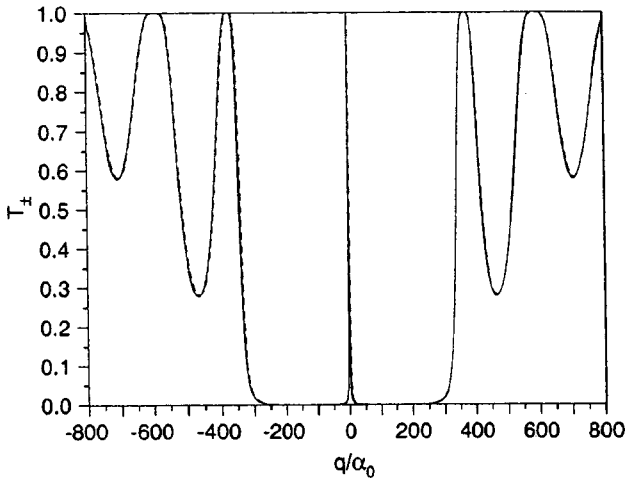

(a)

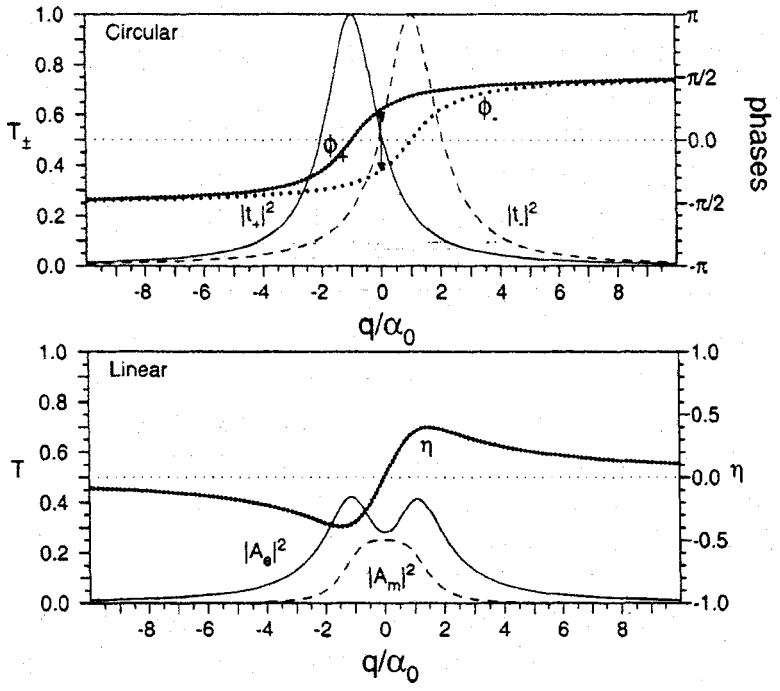

(b)

Fig. 3. Response of a symmetric grating with a central π phase shift. $\kappa = 123, \alpha_0 = 0.47, \alpha_1 = 0.626, L = 0.0252$. (a) Transmission $|t_+|^2$ (solid) and $|t_-|^2$ (dashed). (b) Upper panel: blowup of (a) including phase profiles ϕ_+ (fine dotted) and ϕ_- (coarse dotted). Lower panel: Transmission of linearly polarized modes $|A_e|^2$ (solid), $|A_m|^2$ (dashed), ellipticity η (dotted).

$j \ll k$ and $\kappa_1 = \kappa_2$. Type II systems have no magnetic layers in the rear section: $(N_1M)^j(N_2N_1)^k$. This permits the use of higher index contrast in the rear section (i.e., $\kappa_1 < \kappa_2$), reducing the total length of the device while achieving essentially the same effects. The same separation into Types I and II can be made for corrugated waveguides.

A. Type I Structures

We first consider the Type I system in which $\kappa_1 = \kappa_2 = \kappa$. For the remainder of the paper we neglect the influence of the periodic magnetic factor α_1 on the coupling strengths $\kappa_\pm$ and take $\kappa_\pm = \kappa$. This is an especially good approximation here, where since the reflectivity is very close to unity, variations in the exact coupling strength have a negligible effect. In contrast, this effect is somewhat important in transmission problems [5]. With our assumption that the rear grating is very strong, we can make the approximation that no light is transmitted. In solving the coupled-mode equations (5) we impose this condition by allowing only decaying solutions in the rear grating; the coefficients of any growing solutions are set to zero. With this approximation, we obtain an analytic solution for the reflection coefficient of a single component inside the bandgap

$$r_\pm = \frac{i\sigma - q_\pm}{\kappa} \frac{\sinh(\sigma L_1) - i\sigma/(2q_\pm)\exp(-\sigma L_1)}{\sinh(\sigma L_1) + i\sigma/(2q_\pm)\exp(-\sigma L_1)} \tag{15}$$

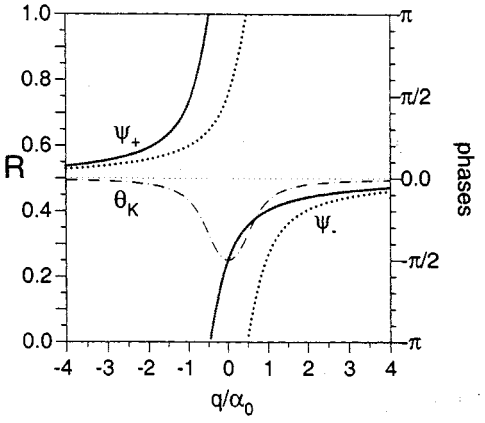

Fig. 4. Enhancement of rotation in reflection for a Type I structure with $\kappa_1 = 123$, $\alpha_0 = 0.47$, and length $L_1 = 0.023$ chosen to obtain -90° rotation at $q = 0$. Line styles are ψ_+ (fine dotted), ψ_- (coarse dotted), and $\overline{\theta}_K = \pi - \theta_K$ (dot-dashed).

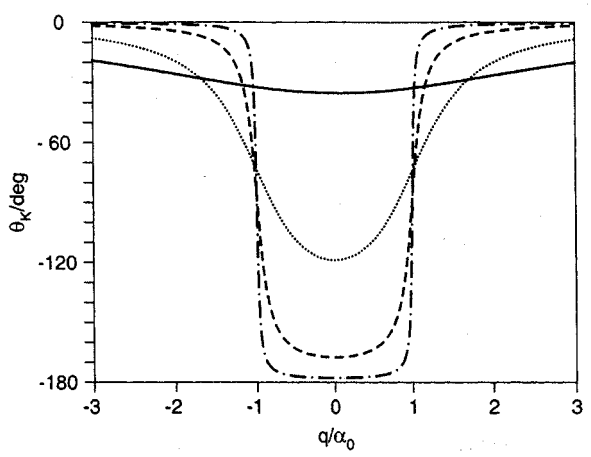

Fig. 5. Rotation as a function of q/α_0 for lengths $L_1 = 1.83$ μm (solid), 2.52 μm (dotted), 3.22 μm (dashed), and 3.91 μm (dot-dashed). Other parameters are as for Fig. 4.

where $\sigma = \sqrt{\kappa^2 - q_\pm^2}$. As the rear grating is a perfect reflector, $r_\pm$ has no dependence on L_2. Fig. 4 shows the typical form of the reflection coefficients, in an analogous fashion to the transmission results studied in Fig. 3. Inside the bandgap, $|r_\pm| \approx 1$ to an excellent approximation, so we do not plot the amplitudes. The phase functions $\psi_\pm$ obtained from (15) are shown as the dotted lines in Fig. 4 (fine dotted for ψ_+, coarse dotted for ψ_-). They have a step-like profile centered around the points $q_\pm = 0$ with the usual magnetic splitting of $2\alpha_0$. This is the remaining signature of the defect, which still persists though the transmission resonance has vanished. Now by (15), we see that near the center of the gap ($|q_\pm| \ll \kappa$), both circular components are equally reflected with $|r_+| = |r_-|$. Thus the reflected light is linearly polarized with zero ellipticity and a rotation θ_K given by (11). Across the resonance shown in Fig. 4, the rotation varies smoothly from zero to a maximum value of $\approx -90^\circ$ at $q/\alpha_0 = 0$.

The rotation angle is shown as a function of q for a variety of lengths in Fig. 5, For shorter lengths L_1 (solid line), moderate rotations of 20°–30° occur over a large bandwidth. For larger lengths (dashed and dot-dashed lines), the central part of the spectrum tends toward experiencing a simple π phase shift (rotation of 180°), and large rotations of $\approx$90° are only found for $q \approx \pm\alpha_0$. For such a configuration, the phase profiles in Fig. 4 are no longer smoothly rising but have become discrete step profiles.

Concentrating just on the rotation at $q = 0$, and assuming $\kappa \gg \alpha_0$ in (15), we use (11) to obtain the rotation

$$\theta_K(q=0) = -\frac{\alpha_0}{\kappa} + 2\tan^{-1}\left(\frac{\kappa \exp(-\kappa L_1)}{2\alpha_0 \sinh \kappa L_1}\right). \qquad (16)$$

In Fig. 6 we plot $\overline{\theta}_K = \pi - \theta_K$ for a structure with $\kappa = 123$ and $\alpha_0 = 0.47$, $\alpha_1 = 0.626$. (Plotting $\overline{\theta}_K$ rather than θ_K removes an unimportant global π phase delay.) The rotation given by (16) is indistinguishable from the exact numerical result shown. Consistent with the curves in Fig. 5, the rotation increases monotonically with the strength of the front grating κL_1. This is associated with the phase functions $\psi_\pm$ becoming more step-like

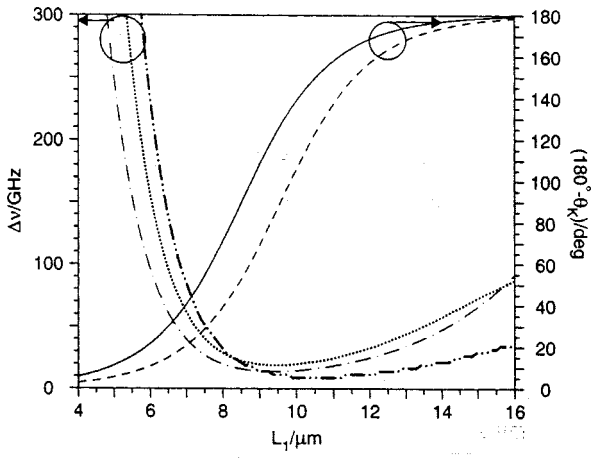

Fig. 6. Rotation $\overline{\theta}_K = 180^\circ - \theta_K$ as a function of the first grating length L_1 (solid line) and 1° bandwidths according to numerical measurement (dotted) and analytic estimate (dot-dashed) for a Type I structure. The dashed and double-dot-dashed lines show the rotation and bandwidth for a corresponding Type II structure. Parameters are $\kappa = 123$ and $\alpha_0 = 0.47$, $\alpha_1 = 0.626$.

around the points $q_\pm = 0$ in Fig. 4 so that the phase difference at $q = 0$ increases. Eventually, however, the increase in phase for each component becomes a discrete step function at the points $q_\pm = 0$. Once this happens, the phase difference $\psi_+ - \psi_-$ at $q = 0$ is fixed at a maximum of 2π and the reflected light experiences a simple phase shift of 180° rather than a rotation. Therefore, the rotation shown in Fig. 6 levels off at 180°.

Note, finally, from Fig. 5 also that there is always a stationary point in the rotation at $q = 0$, and hence the largest bandwidth is obtained by choosing L_1 such that the desired rotation occurs at $q = 0$. In fact, using a Taylor expansion around $q = 0$ in (16), we can find an estimate of the bandwidth Δq over which the rotation varies by less than a desired limit $\delta\theta_K$

$$\delta q = \sqrt{\frac{\delta\theta_K}{\alpha_0 \kappa}} \frac{\kappa^2 + \alpha_0^2 \exp(4\kappa L_1)}{\exp 3\kappa L_1}. \qquad (17)$$

This bandwidth $\Delta\nu = c/(2\pi\overline{n})\,\delta q$ is shown in Fig. 6 for $\delta\theta_K = 1^\circ$ as the dot-dashed line. The dotted line indicates the numerical calculation of the bandwidth.

B. Type II Structures

Equation (16) applies to a periodic structure with the same properties on either side of the defect (Type I). It is also fruitful to consider a second class of structures (Type II), for which a different grating structure is used behind the phase shift. This can have a number of advantages. One can choose a rear grating with higher index contrast, allowing a shorter total system. For example, for the Type I structure considered in Fig. 6, we obtained 90° rotation with a first grating length of only $L_1 = 9$ μm. However, the total structure would have a length of order 30 μm in order to satisfy the condition that the rear grating be stronger than the first. A stronger rear grating could reduce this length by a factor 2. Moreover, if the magnetic material is located only at the front, any applied magnetic field used for switching the rotation can be localized to a smaller region. For Type II structures, the relation corresponding to (16) becomes

$$\theta_K = -\frac{\alpha_0}{\kappa} + 2\tan^{-1}\left(\frac{2\kappa\exp(-\kappa L_1)}{\alpha_0[2\sinh(\kappa L_1) - \exp(-\kappa L_1)]}\right). \tag{18}$$

Note again that as the rear grating is assumed to be a perfect reflector, the rotation θ_K depends on neither the mean index, length, or strength of the rear grating. The only condition [implied by (14)] is that $\kappa_2 L_2 - \kappa_1 L_1 \gtrsim 3$–4. As there is less magnetic material present, the rotation induced by a given length L_1 is somewhat smaller than for the Type I design; from (16) and (18) we see that the same rotation is achieved at $q = 0$ when

$$L_1^{\mathrm{II}} = L_1^{\mathrm{I}} + \frac{\ln 2}{2\kappa} \tag{19}$$

where the superscripts indicate Type I or II. This modest increase in length of the front section can be more than compensated for by choosing a much shorter and stronger rear grating. The dashed and double-dot-dashed lines in Fig. 6 show the rotation and bandwidth, respectively, for a YIG/GGG Type II structure. It is apparent that there is a simple shift in L_1 required for the same rotation. The bandwidth for a given rotation is, however, somewhat reduced.

C. Discrete Stacks and Waveguides

In Fig. 7, we show the enhancement that is possible for a range of different geometries using Bi-YIG as the magnetic material with Type I and II structures. The rotation at $q = 0$ is plotted as a function of the length L of that part of the structure containing magnetic material. Thus for Type I structures, L is the total length; for Type II structures, $L = L_1$ and the total length might typically be of order $1.5L_1$. As mentioned earlier, the length of the structure containing magnetic material is of interest for switching purposes.

The straight line in Fig. 7 indicates the rotation that would be obtained by reflection from a uniform layer of YIG with a strongly reflecting dielectric mirror behind it. This is simply $\theta_K = 2\gamma_0 L$. The rotation induced by our structures must be much higher than this line to be of interest. The two dotted lines

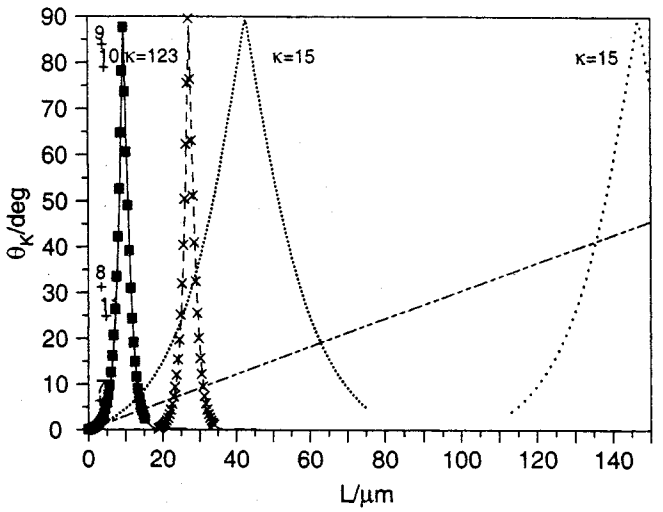

Fig. 7. Rotation as a function of length L. Line styles are solid ($\kappa = 123$, Type II), dashed ($\kappa = 123$, Type I) , fine dotted ($\kappa = 15$, Type II), coarse dotted ($\kappa = 15$, Type I), dot-dashed (uniform magnetic medium). Symbols denote discrete stacks of YIG/GGG (squares and crosses), and YIG/SiO_2 (plus signs).

for which $\kappa = 15$ give the rotation achievable in a typical corrugated slab waveguide for Type I (coarse dotted) and Type II (fine dotted) structures. For these cases, the enhancement of rotation over the uniform material is rather modest due to the limited grating strength that can be attained by surface corrugation.

The solid (Type II) and dashed (Type I) lines for $\kappa = 123$ correspond to YIG/GGG quarter-wave thin-film stacks. The Type II design allows a 90° rotation with the magnetic YIG confined to just 10 μm and a total length of under 20 μm. For these structures, the stacks are sufficiently short that their discrete nature is apparent—there is a significant change in rotation with the addition of a single pair of layers. The squares and crosses indicate individual realizations of the stacks in one unit increments. The points at the Type II and Type I peaks have 22 and 25 layer pairs in front of the defect, respectively. We emphasize that for all these points, the reflectivity exceeds 99% and that it could be increased further by adding additional layers to the rear of the structure. Note also that the strength of the *rear* gratings were held constant in all these calculations. Consistent with (16) and (18), the Kerr rotation depends only on the properties of the front grating, providing only that the rear grating always exceeds the strength of the first sufficiently.

Finally, the plus signs denote Type II YIG/SiO_2 stacks with the number of layers indicated by the adjacent numbers. These stacks show rotations up to 90° with front grating lengths of $\approx$8 μm and total stack lengths of order 15 μm, still with reflectivity over 99%. It is clear that with the large index difference of this system, enormous enhancement in rotation is possible with essentially perfect reflection. Due to the high index contrast, however, significant jumps in rotation occur with the addition of a single layer (compare the points marked 8 and 9, or 10 and 11). If intermediate values of rotation are required, fine-tuning can be achieved by careful selection of the index of the medium in front of the stack or by slight doping of the SiO_2

layers to change the refractive index. This idea is discussed in detail in [5]. All calculations here assumed an input medium with $n = 2.05$, the same as the YIG/GGG stacks.

V. Conclusion

We have examined the problem of achieving high Kerr rotations in periodic stacks without suffering an accompanying loss in reflectivity. The key to optimization is the introduction of an extra degree of freedom by allowing the location of the defect to vary. The rear grating is made sufficiently long to guarantee reflection, and the length of the front grating is then tuned to obtain the desired rotation. The two parts of the structure thus serve two complementary and largely separate roles which simplifies the task of optimization for a particular angle.

References

[1] M. Levy, R. Osgood, Jr, A. Kumar, and H. Bakhru, "Epitaxial liftoff of thin oxide layers: Yttrium iron garnets onto GaAs," *Appl. Phys. Lett.*, vol. 71, pp. 2617–2619, 1997.
[2] M. Inoue, K. Arai, T. Fujii, and M. Abe, "Magnetooptical properties of one-dimensional photonic crystals composed of magnetic and dielectric layers," *J. Appl. Phys.*, vol. 83, pp. 6768–6770, 1998.
[3] ——, "One-dimensional magnetophotonic crystals," *J. Appl. Phys*, vol. 85, pp. 5768–5770, 1999.
[4] S. Sakaguchi and N. Sugimoto, "Transmission properties of multilayer films composed of magnetooptical and dielectric materials," *J. Lightwave Technol.*, vol. 17, pp. 1087–1092, 1999.
[5] M. J. Steel, M. Levy, and R. M. Osgood Jr., "High transmission enhanced Faraday rotation in one-dimensional photonic crystals with defects," *IEEE Photon. Technol. Lett.*, submitted for publication.
[6] ——, "Photonic band gaps with defects and the enhancement of Faraday rotation," *J. Lightwave Technol.*, vol. 18, pp. 1297–1308, Sept. 2000.
[7] M. Inoue and T. Fujii, "A theoretical analysis of magnetooptical Farday effect of YIG films with random multilayer structures," *J. Appl. Phys.*, vol. 81, pp. 5659–5661, 1997.
[8] R. Kashyap, *Fiber Bragg Gratings*. San Diego, CA: Academic, 1999.
[9] J. D. Joannopoulos, R. D. Meade, and J. N. Winn, *Photonic Crystals: Molding the Flow of Light*. Princeton, NJ: Princeton Univ. Press, 1995.
[10] M. Born and E. Wolf, *Principles of Optics*. Oxford, U.K.: Pergamon, 1989.

M. J. Steel, photograph and biography not available at the time of publication.

M. Levy, photograph and biography not available at the time of publication.

R. M. Osgood, Jr. (SM'82–F'87), photograph and biography not available at the time of publication.